Dovepress
Taylor & Francis Group

ORIGINAL RESEARCH

Design, Synthesis, and Biological Evaluation of Novel Hydroxytyrosol Derivatives as Protectors for Vascular Endothelium Against Lipid Overload

Xi-Xi Hou[1,2,*], Shuang Wang[1,3,*], Xiao-Xia Ma[1,2,*], Ying Wen[1,3,*], Zhi-Jun Li[4], Xu-Yun Liu[5], Xing Zhang[3], Yang Zhang [6], Xiang-Yang Qin[2]

[1]College of Life Sciences, Northwest University, Xi'an, People's Republic of China; [2]Department of Chemistry, School of Pharmacy, Fourth Military Medical University, Xi'an, People's Republic of China; [3]Department of Recuperation and rehabilitation for flight personnel, School of aerospace medicine, fourth Military Medical University, Xi'an, People's Republic of China; [4]School of Chemistry and Chemical Engineering, Shaanxi University of Science and Technology, Xi'an, People's Republic of China; [5]Center for Mitochondrial Biology and Medicine, the Key Laboratory of Biomedical Information Engineering of Ministry of Education, School of Life Science and Technology, Xi'an Jiao Tong University, Xi'an, People's Republic of China; [6]Department of Medical Electronics, School of Biomedical Engineering, Fourth Military Medical University, Xi'an, People's Republic of China

*These authors contributed equally to this work

Correspondence: Xu-Yun Liu, Center for Mitochondrial Biology and Medicine, the Key Laboratory of Biomedical Information Engineering of Ministry of Education, School of Life Science and Technology, Xi'an Jiao tong University, Xi'an, Shaanxi Province, 710049, People's Republic of China, Email xuyunliu@xjtu.edu.cn; Xiang-Yang Qin, Department of Chemistry, School of Pharmacy, Fourth Military Medical University, Xi'an, Shaanxi Province, 710032, People's Republic of China, Email qinxiangyang@fmmu.edu.cn

Background and Objective: Hydroxytyrosol (HT) is reported to protect endothelial cells against metabolic overload through inhibiting inflammation. However, the hydrophilic nature of HT limits its oral bioavailability and biological efficiency. The aim of the study was to design and synthesize novel hybrid molecules to improve HT's biological efficiency.

Materials and Methods: A pharmacophore connection strategy was used to design and synthesize novel hybrid molecules by combining HT or its analogues with adamantane (ADM). Palmitic acid (PA) was used to induce lipid overload in HAEC cells, and P407 was used to induce acute hyperlipidemia in C57 mice.

Results: We found that DP-ADM, combining ADM and dopamine (a HT analogues), exhibited potent protective effects against metabolic overload-induced endothelial dysfunction. DP-ADM showed low toxicity and inhibited inflammation in response to PA overload in cultured endothelial cells. Additionally, it (30 mg/kg) decreased circulating lipids to an extent similar to HT in a mouse model of hyperlipidemia and was superior to HT in decreasing circulating inflammatory cytokine. It was also superior to HT in improving vascular endothelial function in mice with hyperlipidemia. Mechanistically, DP-ADM inactivated MAPK signaling, as evidenced by downregulated phosphorylation of p38 and Erk. Inhibition of MAPK or NF-κB abolished the anti-inflammatory effect of DP-ADM. Specifically, DP-ADM activated FoxO1 signaling and increased mitochondrial biogenesis in endothelial cells.

Conclusion: Overall, DP-ADM is a superior form of HT, highlighting its potential therapeutic use in improving endothelial function in metabolic diseases.

Keywords: hydroxytyrosol derivatives, endothelial function, lipid overload, MAPK, inflammation

Introduction

As a highly dynamic monolayer of cells lining the vascular network, the endothelium plays a crucial role in maintaining systemic physiological function. Endothelial cells are continuously exposed to various circulating factors and pathogenic stimuli that lead to endothelial damage and cellular senescence.[1] A growing body of literature suggests that endothelial cell damage and senescence are significant contributors to multiple cardiovascular and metabolic diseases, including atherosclerosis, heart failure, hypertension, obesity, and diabetes.[2–4] Emerging evidence indicates that metabolic

Graphical Abstract
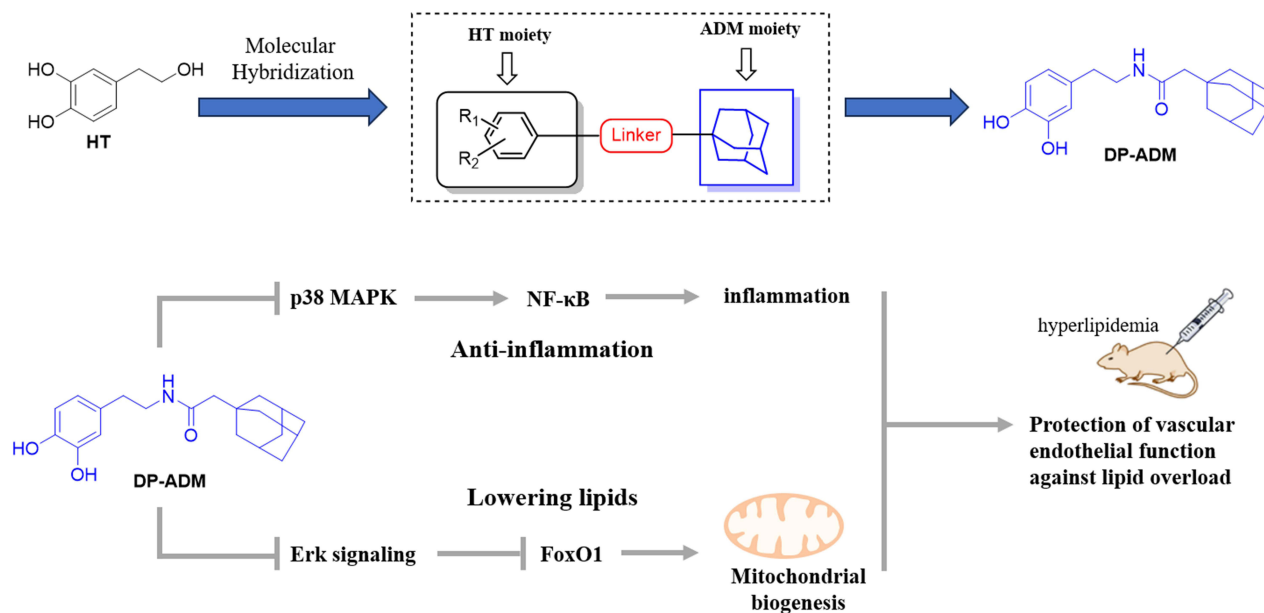
overload, particularly hyperlipidemia, is a major contributor to endothelial dysfunction.[5–7] Therefore, it is of great theoretical and practical significance to develop innovative drugs for preventing endothelial injury from metabolic overload.[8,9]

Hydroxytyrosol (HT) [IUPAC name: 4-(2-Hydroxyethyl)-1,2-benzenediol] (Figure 1) is a natural phenolic compound found in olive fruits, branches, leaves or grapes and wines, exhibiting anti-inflammatory, anti-atherogenic, anti-oxidative and anti-thrombotic activities.[10,11] The protective effects of HT against endothelial cell dysfunction and lipid metabolic disorder have been reported.[12–14] However, the hydrophilic nature of HT strongly limits its oral bioavailability due to insufficient uptake from the mucosa, resulting from its poor epithelial permeability.[15,16] Additionally, phenolic compounds are unstable in air and oxygen.[17] Therefore, to fully exploit its health benefits, the search for novel derivatives and analogues of HT with greater stability, improved availability, and pharmacological activities is of interest to medicinal chemists. Adamantane (ADM), a rich natural pharmacophore, has a notable impact in the therapeutic field due to its "add-on" lipophilicity to any pharmacophoric moieties, allowing adamantane-based compounds to pass through cell membranes. Adding an adamantane unit improves the absorption, distribution, metabolism and excretion properties of the novel molecule.[18] ADM-based structurally modified compounds have been found to have a broad range of applications in the pharmaceutical field. A series of commercially available drugs, including adapromine (antiviral),
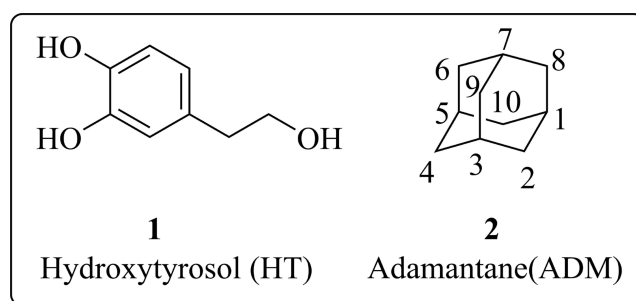

Figure 1 The structure of HT and ADM.

adapalene (for acne treatment), saxagliptin (antidiabetic), bromantane (anxiolytic), and memantine (anti-Alzheimer), contain an adamantane moiety (Figure 2).[19] Furthermore, compound 77 containing adamantane have been shown to exhibit anti-inflammatory properties (Figure 2).[20] Therefore, in this study, we chose adamantane to improve the lipophilicity of hydroxytyrosol and achieve a synergistic effect through molecular hybridization.

Hybrid molecules, in which one pharmacophore is attached to another into a single molecule, have the potential to increase affinity, enhancing efficacy, and improving safety.[21] Nowadays, hybrid drugs have garnered interest for the purposeful and logical design of novel molecules with improved pharmacological potency.[22] It has been reported that hybrid molecules can reduce endothelial dysfunction.[23] The aim of the present work was to design, synthesize and evaluate novel HT derivatives to protect vascular endothelial cells against metabolic overload. Hybrid molecules were achieved using two strategies, (a) combining drug pharmacophoric moieties and (b) combining two or more entire drugs.[22] In this work, we used a direct connection strategy to design and synthesize novel hybrid molecules, ADM-based HT agents, by combining ADM and HT analogues (Figure 3). These hybrid molecules consist of two entire medications joined through a covalent linker of appropriate length via ester or amide bonds. Dopamine, also known as 3-hydroxytyramine, is a natural phenolic compound largely secreted by the basal ganglia of the brain.[24,25] Dopamine is structurally different from hydroxytyrosol, with only an amino group and a hydroxyl group. Therefore, to compare the effects of amide and ester bonds on pharmacological activity, we chose dopamine as a HT analogue. We found that DP-ADM, combining ADM and dopamine (a HT analogues), exhibited potent protective effects against metabolic overload-induced endothelial dysfunction, highlighting its potential therapeutic use for vascular diseases.

Materials and Methods
Chemistry
All reactions were monitored by TLC on 0.25 mm silica gel 60-F plates. The extracts were dried with Na_2SO_4. Flash chromatography was carried out in silica gel (300–400 mesh). Yields referred to chromatographically and spectroscopically pure materials, unless otherwise stated. All reagents were used as supplied by Adamas and Energy chemicals. Dichloromethane (DCM) was distilled from calcium hydride; tetrahydrofuran was distilled from sodium/benzophenone.
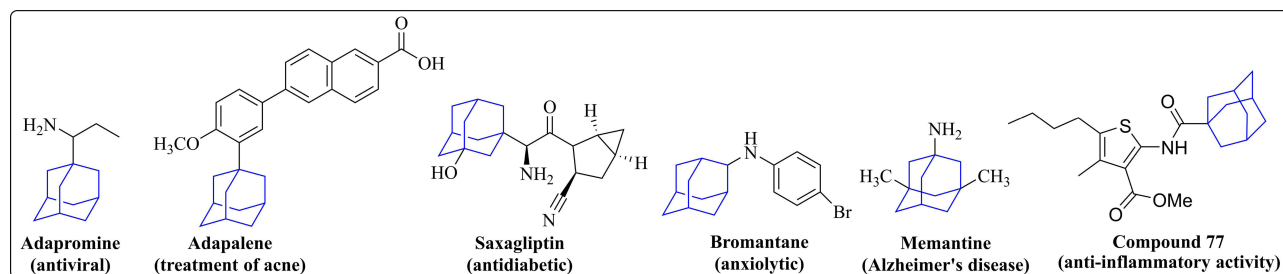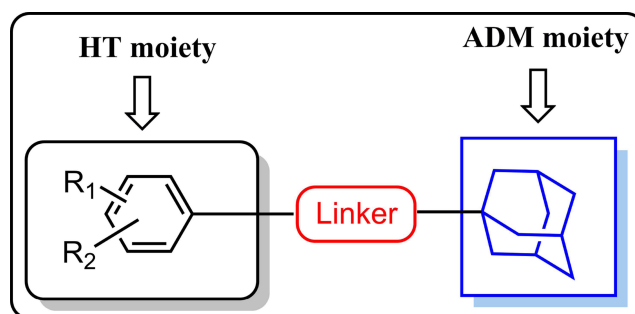

Figure 2 Adamantane-based drugs.

Figure 3 Structural design of novel hybrid molecules of HT and ADM.

All reactions were carried out in oven-dried glassware under a nitrogen atmosphere unless otherwise noted. (Nuclear magnetic resonance) NMR spectra were recorded on a Bruker ASCEND^{TM} 600 spectrometers (Bruker, USA) at ambient temperature with $CDCl_3$ as the solvent unless otherwise stated. Chemical shifts (d) were expressed in parts per million relatives to chloroform (^1H, d 7.26; ^{13}C, d 77.16). Multiplicities of NMR signals were expressed as s (singlet), d (doublet), t (triplet), q (quartet), m (multiplet) and coupling constants. High resolution mass spectroscopy (HRMS) was carried out on an AB SCIEX X500R QTOF (AB SCIEX, USA) instrument. All melting points were measured on a Buchi Melting Point M-565 apparatus. Infrared (IR) spectra were recorded on a Thermo Fisher Nicolet IS50. The purity of all tested compounds was determined to be more than 95% using HP Agilent 1260 infinity HPLC instrument.

Synthesis of 3.4-Dihydroxyphenethyl 2-(Adamantan-1-Yl) Acetate (HT-ADM)

A mixture of 4-(2-hydroxyethyl) benzene-1,2-diol (308.33 mg, 2.0 mmol, 1 eq), imidazole (408.47 mg, 6 mmol, 3 eq), and TBDMSCl, tert-butyldimethylsilyl chloride (753.61 mg, 5 mmol, 2.5 eq) was dissolved in DMF (2 mL). The resulting mixture was stirred at room temperature for 3 h. The completion of the reaction was monitored by TLC analysis. After that, the mixture was diluted with water (20 mL) and extracted with ethyl acetate (20 mL × 3). The organic phases were combined, washed with brine (20 mL), dried with Na_2SO_4, filtered and concentrated. The crude product was purified by flash column chromatography on silica gel (PE/EtOAc=100:1, v/v). This process yielded a colorless oil **1** (693.7 mg, 90.6% yield). Rf = 0.2 (PE:EtOAc = 100:1, v/v); HRMS(ESI) m/z: [M+H]$^+$ calculated for $C_{20}H_{38}O_3Si_2$ 383.2432; found 383.2432. This product can then be used in next step without further purification. (Figure S1 in the Supplementary Materials).

Adamantane acetic acid (ADMAA, 495.6 mg, 2.5 mmol, 1 eq) was dissolved in dry DCM (6 mL). A drop of DMF was added, and then oxalyl chloride (0.25 mL, 3 mmol, 1.2 eq) was slowly added dropwise at 0 °C. The resulting mixture was stirred for 2 h, followed by concentration under vacuum to remove the excess oxalyl chloride. The obtained product was 2-(adamantan-2-yl) acetyl chloride **2**, which can then be used in the next step without further purification.

A solution of compound **2** (115.5 mg, 0.21 mmol, 1 eq) and DMAP (148.16 mg, 1.19 mmol, 1.2 eq) in dry THF (14 mL) was prepared under nitrogen. The freshly prepared compound **1** was added dropwise to the mixture and stirred at room temperature for 4 h. The completion of the reaction was monitored by TLC analysis. The mixture was then diluted with water (20 mL) and extracted with ethyl acetate (20 mL × 3). The organic phases were combined, washed with brine (20 mL), dried with Na_2SO_4, filtered, and concentrated. The crude product was purified by flash column chromatography on silica gel (PE:EtOAc=100:1, v/v). This process yielded a light-yellow oil **3** (504.5 mg, 91.12% yield). Rf = 0.35 (PE: EtOAc=100:1, v/v); HRMS(ESI) m/z: [M+H] + calculated for $C_{32}H_{54}O_4Si_2$ 559.3633; found 559.3633. (Figure S2 in the Supplementary Materials).

A suspension of compound **3** (379 mg, 0.99 mmol, 1 eq) was dissolved in 2 mL of dry THF. Then, TBAF (0.45 mL, 0.45 mmol, 2.2 eq) and acetic acid (0.4 mL, 10.33 mmol, 50 eq) were slowly added dropwise to the mixture at 0 °C and stirred for 3 h at the same temperature. The progress of the reaction was monitored using TLC analysis to determine its completion. Subsequently, the mixture was diluted with 20 mL of water and extracted three times with ethyl acetate. The organic phases were combined, washed once with a sodium bicarbonate solution, dried with Na_2SO_4, filtered, and concentrated. The resulting crude product was purified by flash column chromatography on silica gel using a (PE: EtOAc=5:1, v/v) solvent system. This process yielded a light-yellow oil **HT-ADM** (54.2 mg, 79.38% yield). The structural identification data are shown below: HPLC purity (99.76%); Rf = 0.3 (PE: EA = 5:1); ^1H NMR (600 MHz, $CDCl_3$) δ 6.79 (d, J = 8.0 hz, 1H), 6.75 (d, J = 1.8 hz, 1H), 6.64 (dd, J = 8.1, 1.8 hz, 1H), 4.24 (t, J = 7.1 hz, 2H), 2.82 (t, J = 7.1 hz, 2H), 2.05 (s, 2H), 1.93 (s, 3H), 1.67 (d, J = 12.1 hz, 3H), 1.59 (d, J = 11.6 hz, 3H), 1.54 (d, J = 2.0 hz, 6H); ^{13}C NMR (151 MHz, $CDCl_3$) δ 172.76, 143.78, 142.48, 130.67, 121.42, 115.97, 115.42, 64.99, 49.27, 42.50, 36.79, 34.59, 32.94, 28.71. IR (neat): 3360, 2899, 2847, 1697, 1605, 1257, 1194 cm^{-1}. HRMS(ESI) m/z: [M-H] $^-$ calculated for $C_{20}H_{26}O_4$ 329.1758; found 329.1736. (Figures S3–S5 and S15 in the Supplementary Materials).

Synthesis of 2-(Adamantan-1-Yl)-N-(3,4-Dihydroxyphenethyl) Acetamide (DP-ADM)

A suspension of compound **ADMAA**, Adamantan-1-amine (237.89 mg, 1.2 mmol, 1.2 eq), HOBT (206.83 mg, 1.5 mmol, 1.5 eq), and EDCI (234.74 mg, 1.2 mmol, 1.2 eq) was dissolved in 5 mL of dry DCM under a nitrogen

atmosphere. Separately, a solution of dopamine hydrochloride (189.64 mg, 1 mmol, 1 eq) and triethylamine (0.49 mL, 3.5 mmol, 3.5 eq) in 2 mL of dry dichloromethane was slowly added dropwise to the mixture at 0 °C. The resulting solution was stirred for 0.5 h at 0 °C and then allowed to reach room temperature, where it was stirred overnight. The progress of the reaction was monitored using TLC analysis to determine its completion. The DCM layer was removed, and the remaining solution was diluted with 20 mL of water and extracted three times with ethyl acetate. The organic phases were combined, washed once with 1 M HCl, followed by a wash with brine. The solution was dried with Na_2SO_4, filtered, and concentrated. The crude product was then purified by flash column chromatography on silica gel using a (PE:EtOAc=2:1, v/v) solvent system.[26] This process yielded a white solid DP-ADM (245.9 mg, 74.64% yield). The structural identification data are shown below: HPLC purity (98.31%); Rf = 0.45 (PE: EA = 2:1); m.p.: 50.8 ~ 62°C; ^{1}H NMR (600 MHz, CDCl$_3$) δ 8.12 (s, 1H), 6.80 (dd, J = 13.1, 4.7 hz, 2H), 6.56 (d, J = 8.0 hz, 1H), 5.61 (t, J = 5.5 hz, 1H), 3.49 (q, J = 6.8 hz, 2H), 2.70 (t, J = 7.1 hz, 2H), 1.92 (s, 3H), 1.90 (s, 2H), 1.85 (s, 1H), 1.66 (d, J = 12.1 hz, 3H), 1.58 (d, J = 11.9 hz, 3H), 1.51 (s, 5H).^{13}C NMR (151 MHz, CDCl$_3$) δ 172.46, 144.61, 143.43, 130.43, 120.49, 115.56, 115.22, 77.37, 77.16, 76.95, 52.02, 42.66, 41.03, 36.74, 35.02, 32.94, 28.70. IR (neat): 3290, 2899, 2845, 1600, 1515, 1445 cm^{-1}. HRMS(ESI) m/z: [M+H]$^+$ calculated for $C_{20}H_{27}NO_3$ 330.2063; found 330.2063. (Figure S6–S8 and S16 in the Supplementary Materials).

Synthesis of (6-((3,4-Dihydroxyphenethyl) amino)-6-Xohexyl) triphenylphosphonium Bromide (DP-TPP)

Compound **4** ((5-carboxypentyl) triphenylphosphonium bromide, TPP) (933.36 mg, 2 mmol, 1 eq) was dissolved in 10 mL of dry DCM. Then, dopamine hydrochloride (370.42 mg, 2.4 mmol, 1.2 eq), DCC (505.31 mg, 2.4 mmol, 1.2 eq), and DMAP (124.66 mg, 1 mmol, 0.5 eq) were added to the mixture at room temperature and stirred. The mixture was stirred at room temperature overnight. TLC analysis was performed to monitor the progress of the reaction until it was deemed complete. The mixture was then filtered and the filtrate was washed with a sodium bicarbonate solution. After drying with Na_2SO_4, the solution was filtered and concentrated. The resulting material was purified using flash column chromatography on silica gel with a DCM/MeOH (10:1, v/v) solvent system. This yielded a white solid **DP-TPP** (316.8 mg, 26.82% yield). The structural identification data are shown below: HPLC purity (96.85%); Rf = 0.4 (DCM: MeOH = 10:1); m.p.: 46.3 ~ 48.7°C; ^{1}H NMR (600 MHz, DMSO) δ 8.76 (s, 1H), 8.68 (s, 1H), 7.91–7.88 (m, 3H), 7.81–7.76 (m, 12H), 6.61 (d, J = 7.9 hz, 1H), 6.55 (d, J = 1.6 hz, 1H), 6.40 (dd, J = 8.0, 1.6 hz, 1H), 5.74 (s, 1H), 3.54 (s, 2H), 3.13 (dd, J = 14.1, 6.5 hz, 2H), 2.47 (t, J = 7.5 hz, 2H), 2.00 (t, J = 7.1 hz, 2H), 1.49 (dd, J = 15.0, 7.6 hz, 4H), 1.41 (d, J = 6.8 hz, 2H); ^{13}C NMR (151 MHz, DMSO) δ 171.83, 145.08, 143.55, 135.00, 134.98, 133.69, 133.62, 130.38, 130.30, 119.28, 118.90, 118.34, 116.04, 115.54, 54.99, 40.54, 40.06, 39.94, 39.80, 39.66, 39.52, 39.38, 39.24, 39.10, 35.09, 34.77, 29.61, 29.50, 24.55, 21.78, 21.75, 20.40, 20.07. IR (neat): 3388, 3056, 2907, 2851, 1636, 1520, 1436 cm^{-1}. HRMS(ESI) m/z: [M-Br]$^+$ calculated for $C_{32}H_{35}BrNO_3P$ 512.2343; found 512.2346. (Figures S9–S11 and S17 in the Supplementary Materials).

Synthesis of N-(Adamantan-1-Yl)-2-(3,4-Dihydroxyphenyl) Acetamide (DOP-ADM)

3.4-Dihydroxyphenylacetic acid **DOPAC** (343.16 mg, 2 mmol, 1 eq) and triethylamine (0.56 mL, 4 mmol, 2 eq) were dissolved in 6.5 mL of DMF and cooled to 0 °C. To the mixture, amantadine **5** (370.42 mg, 2.4 mmol, 1.2 eq) was added, followed by slowly dropwise addition of a dry DCM (9.5 mL) solution of BOP (1.08 g, 2.4 mmol, 1.2 eq). The mixture was stirred at 0 °C for 30 minutes and then brought to room temperature and stirred overnight. TLC analysis was performed to monitor the progress of the reaction until it was deemed complete. The DCM layer was separated, and the solution was diluted with 20 mL of water and extracted three times with ethyl acetate. The organic phases were consolidated and washed with a sodium bicarbonate solution. After drying with Na_2SO_4, the solution was filtered and concentrated. The resulting material was purified using flash column chromatography on silica gel with a PE/EtOAc (1:1, v/v) solvent system. This yielded a white solid **DOP-ADM** [26](129.6 mg, 21.5% yield). The structural identification data are shown below: HPLC purity (99.74%); Rf = 0.3 (PE: EA = 1:1); m.p.: 100.5 ~ 109.2°C; ^{1}H NMR (600 MHz, DMSO) δ 8.72 (s, 2H), 7.36 (s, 1H), 6.64 (d, J = 1.7 hz, 1H), 6.61 (d, J = 8.0 hz, 1H), 6.46 (dd, J = 8.0, 1.7 hz, 1H), 3.12 (s, 2H), 1.98 (s, 3H), 1.89 (s, 6H), 1.59 (s, 6H); ^{13}C NMR (151

MHz, DMSO) δ 170.15, 144.92, 143.69, 127.83, 119.68, 116.33, 115.31, 50.73, 42.65, 41.09, 39.94, 39.80, 39.66, 39.52, 39.38, 39.24, 39.10, 36.13, 28.89. IR (neat): 3457, 3374, 2907, 2851, 1694, 1678, 1602 cm^{-1}. HRMS(ESI) m/z: [M-H]$^-$ calculated for $C_{18}H_{23}NO_3$ 300.1595; found 300.1605. (Figures S12–S14 and S18 in the Supplementary Materials).

Cell Culture and Treatment

Human aorta endothelial cells (HAECs) were purchased from Bio Leaf (Shanghai Bio Leaf Biotech Co., Ltd, Shanghai, China). Cells were cultured in Dulbecco's modified Eagle's medium (DMEM) supplemented with 10% fetal bovine serum,1% penicillin-streptomycin, and 10 μg/mL heparin in a humid environment of 95% air and 5% CO_2. Cells of passage 3–9 were used. Palmitic acid (PA) was dissolved in NaOH at 90°C for 15 min to prepare a 200 mm PA solution. HAECs were pretreated with or without different concentrations of HT and its derivatives (0.01, 0.1, 1, and 10 μM) for 24 h, followed by treatment with 500 μM PA for 24 h. HAECs were pretreated for 30 min with or without the p38 inhibitor SB203580 (10 μM, ab120162, Abcam Inc, Cambs, UK), or Erk inhibitor U0126 (10 μM, 109511–58-2, MedChemExpress, SNJS, USA), or NF-κB inhibitor QNZ (10 μM, 545380–34-5, MedChemExpress, SNJS, USA), treated with or without DP-ADM for 24 h, and followed by treatment with 500 μM PA for 24 h. The protein and RNA were extracted for subsequent experiments.

MTT Assay

Cells were incubated with culture medium containing 500 μM MTT (3-[4,5-dimethylthiazol-2-yl]-2,5 diphenyl tetra-zolium bromide) per well. After incubation for 3 h, dimethyl sulfoxide was added to each well to dissolve the purple crystals sufficiently to stop the reaction. The absorbance (OD value) of the crystal was measured at 570 nm.

qRT-PCR

Total RNA was extracted from cells using TRIzol reagent (15596018, Thermo Fisher Scientific Inc, MA, USA) for reverse transcription into cDNA according to the manufacturer's protocol. Reactions were performed in technical and biological triplicate using a 96-well format on the ABI Step One Plus system according to instructions from the Hieff qPCR SYBR Green Kit (11201; YESEN Biology, Shanghai, China). The qRT-PCR conditions were 95°C for 5 min, followed by 40 cycles of 95°C for 10s and 60°C for 30s. Data were normalized to the mRNA of actin as a housekeeping gene and were analyzed by the $2^{-\Delta\Delta Ct}$ method. The primers used are shown in supplementary material (Table S1).

Detection of Reactive Oxygen Species (ROS)

ROS detection was operated according to the instructions of the ROS detection Kit (S0033S; Beyotime, Shanghai, China).

Detection of mtDNA Copy Number

Total DNA was extracted according to the instructions of the QIAamp DNA Mini Kit (51306; QIAGEN, Germany). The copy number of mtDNA was detected using qRT-PCR with D-loop and 18S rRNA primers (Table S1).

Western Blotting

Cell samples were washed with precooled 4°C phosphate-buffered saline (PBS) and incubated with a solution containing EDTA-free, western and IP lysis buffer (P0013B; Beyotime, Shanghai, China) of 100 × (APT006; AntiProtech, Texas) and phosphatase inhibitor cocktail lysed 100 × (APT008; AntiProtech, Texas, USA). The lysates were homogenized and centrifuged at 13,000 g for 15 min at 4°C, and the supernatants were collected. Then, the concentrations of protein were determined using the BCA protein assay kit (P0009; Beyotime, Shanghai, China). Extracted protein samples (15–30 μg per lane) were subjected to 10% SDS-polyacrylamide gelelectrophoresis (SDS-PAGE; P0012A; Beyotime, Shanghai, China), and protein-containing separation gels were transferred to nitrocellulose membranes (ISEQ00010; Merck Millipore Ltd, Darmstadt, Germany). After electrophoresis for 2–3 h, 5% skim milk/TBST was used for 1–2 h at room temperature. The membranes were incubated with the primary antibodies overnight at 4°C, and then they were incubated with the horseradish peroxidase-conjugated secondary antibodies for 1–2 h at room temperature. Western blot analysis was developed using standard procedures, detected using the Pierce enhanced chemiluminescence Western

blotting detection kit (MI00607A; Mishu, Shanxi, China), and quantified by scanning densitometry. Primary antibodies against phospho-p38 (1:2000, 9216S), phospho-38 (1:1000, 92125S), phospho-NF-κB (1:1000, 3033T), NF-κB (1:1000, 8242S), phospho-Erk (1:1000, 4370S), Erk (1:1000, 4695S), FoxO1 (1:1000, 2880S), phospho-eNOS (1:1000, Ser1177), eNOS (1:1000, 32027S), Mfn2 (1:1000, D2D10), Drp1 (1:1000, 8570S), and β-actin (1:1000, 8H10D10) were all purchased from Cell Signaling Technology (Danvers, MA, USA). Mfn1 (1:1000, sc50330) was purchased from Santa Cruz Biotechnology (Dallas, Texas, USA). Opa1 (1:1000, ab157457) was purchased from Abcam (Cambridge, UK). PGC-1α (1:1000, 66,369-1-1g) was purchased from Proteintech (Wuhan, China). Tubulin (1:1000, A12289) was purchased from Company ABclonal, Inc. (Wuhan, China).

Animal Experiments

Male C57BL6 mice (6–8 weeks old) were obtained from the Animal Center of Fourth Military Medical University. All animal experiments were performed in accordance with the National Institutes of Health guidelines on laboratory animals and approved by the Fourth Military Medical University Animal Care and Use Committee. All animals were housed in animal rooms controlled by temperature (22–28°C) and humidity (60%) and kept in a 12 h light/dark cycle throughout the experiment, with free access to food and water. All animal procedures were approved by Animal Experiment Welfare and Ethics Committee of Fourth Military Medical University. The total number of animals used in the study is approximately 150, which includes those utilized in preliminary experiments to determine dosing as well as in the formal experiments. One week after domestication, mice were randomly divided into the following four groups: control group (n = 8), hyperlipidemia group (n = 8), HT-treated group (n = 8) (30 mg/kg/day HT gavage once a day for 21 days), and DP-ADM-treated group (n= 8) (30 mg/kg/day DP-ADM gavage once a day for 21 days). Acute hyperlipidemia was induced by intraperitoneal injection with P407 (poloxamer 407, Sigma-Aldrich, Darmstadt, Germany) (0.05 g/kg) for exactly 24 h (Day 22), and control mice were given the same volume of sterile saline. All efforts were made to minimize the number and suffering of the animals used in the study. The NEFA (non-esterified fatty acid), TG (triglyceride), TC (total cholesterol), LDL-c (low-density lipoprotein cholesterol), HDL-c (high-density lipoprotein cholesterol), NO, IL-6 (interleukin 6), and TNF-α (tumor necrosis factor-α) contents in serum or thoracic aortas were analyzed following instructions of kits (A042-2-1, A110-1-1, A111-1-1, A113-1-1, A112-1-1 and A013-2-1, Jiancheng Biochemical Inc. Ltd., Nanjing, China) and (E-EL-M0044c, E-EL-M3063, Elabscience, Wuhan, China).

Detection of Vasodilatation

The mice were anesthetized with sodium pentobarbital (200 mg/kg, i.p) and sacrificed. The thoracic aortas were excised and placed in a precooled PSS solution (NaCl, 69.5 g; KCl, 3.5 g; $CaCl_2$, 2.27g; $MgSO_4.7 H_2O$, 2.9 g; $NaHCO_3$, 21 g; KH_2PO_4, 1.6 g; Glucose, 10.9 g dissolved in 1 L of water). During dissection, the thoracic aortas were cut into 1 mm rings, which was then mounted in a myographic system (DMT 610M, Danish Myo Technology, Denmark). At the same time, they were incubated in PSS solution at 37°C (PH 7.35–7.45) by continuous injection of a mixture gas of 5% CO_2 and 95% O_2. The thoracic aorta was subjected to natural resting tension, equilibrated for 40 min, and the aortic segment was precontracted with prostaglandin H_2 /thromboxane A_2 receptor agonist (U46619, 56,985–40-1, APExBIO Technology LLC, USA) (10 μM), and cumulatively added ACh (acetylcholine) (60–31-1, Sigma-aldrich) (10^{-8}-10^{-3} M) to induce vasodilatation. The percentage of thoracic aortic contractility induced by U46619 counteracts the effect of ACh to quantify vasodilatation.

H&E Staining

The isolated thoracic aortas were fixed with 4% paraformaldehyde for 48 h. Subsequently, the samples were dehydrated and embedded in paraffin. They were then sliced into 3 μm slices using a Leica RM-2165 microtome (Leica, Bensheim). After baking in the oven for 2 h, paraffin wax was put into xylene and alcohol for gradient dewaxing. The paraffin sections were then stained with hematoxylin for 0.5–1 min, rinsed with water, and then returned to blue with 1% ammonia solution for 1 min, followed by rinsing with running water for several seconds. The sections were then dipped in eosin dye for a few seconds and rinsed with running water. The paraffin sections were made transparent by placing them into ethanol and xylene, and finally mounted in neutral balsam. The histopathology images were acquired using

a Nikon E200 optical microscope (Nikon, Tokyo, Japan). The thickness of thoracic aorta was quantified using ImageJ software.

Immunofluorescence Staining

HAECs were fixed with 4% paraformaldehyde at room temperature for 30 min in the dark. After fixation, cells were washed three times with PBS with shaking and permeabilized with 0.2% Triton X-100 (Sigma). After blocking with BSA for 1 h, the cells were incubated with anti-rabbit-FoxO1 antibody (CST, Beverly, MA, USA). After rinsing with PBS, plates were incubated with Alexa Fluor 555-conjugated anti-rabbit IgG (Invitrogen, Carlsbad, CA, USA) antibodies. Cells were then washed three times with PBS, stained with DAPI (Invitrogen, Carlsbad, CA, USA) for 10–20 min, rinsed once with PBS, and then immunofluorescence images were obtained using an inverted confocal microscope (Zeiss LSM 800).

Statistical Analyses

All values are expressed as mean ± SD, unless otherwise specified. The normality of the data distribution was assessed using the Kolmogorov–Smirnov normality test. These analyses were conducted using SPSS statistical software. Data were compared using either one-way or two-way ANOVA, with all ANOVA tests followed by an unpaired t-test as appropriate. Bonferroni correction for multiple comparisons was applied. Differences were considered statistically significant at $P < 0.05$.

Results and Discussion

Chemistry

The Synthesis of the Ester Hybrid Molecules

Ester bonding is a widely applied and common strategy for drug design, which is to mask polar functionalities such as alcohols or carboxylic acids by turning them into esters, thus improving cell permeability.[27] Many marketed drugs contain ester bonds, such as Enalapril, Benazepril, Quinapril, Cilazapril, Moexipril.[28] With the strategy of drug design, we designed and synthesized the first type of hybrid molecules by ester bond coupling between HT and Adamantane acetic acid. The phenolic hydroxyl group of HT was protected by the TBS group. To increase the reactivity of Adamantane acetic acid, it was first converted to acyl chloride **2**. Then, the acyl chloride **2** with TBS protected hydroxytyrosol **1** was treated with 4-dimethylaminopyridine (DMAP) in dry THF at room temperature to afford amide **3** in 91.1% yield. The TBS protecting group was removed to afford the required product **HT-ADM** in TBAF and AcOH conditions[29] (Scheme 1).

The Synthesis of the Amide Hybrid Molecules

The amide bond plays a major role in the elaboration and composition of biological systems. Amides are recognized as the key functional group found in peptides, polymers, and many natural products and pharmaceuticals.[30] Indeed, according to a medicinal chemistry database, more than 25% of the natural and synthetic pharmaceutical drugs on the market contain one or more amide functional groups as a core structural motif.[30] In this section, we designed and synthesized eleven hydroxytyrosol derivatives containing amide bond through the condensation of a carboxylic acid with
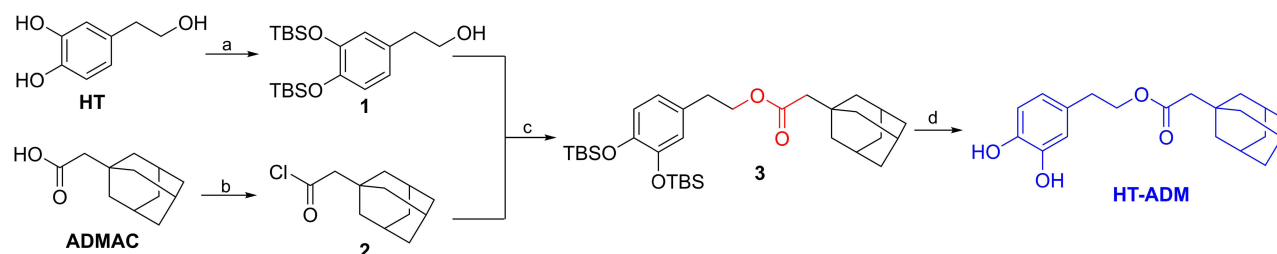

Scheme I Reagent and condition: (a) Imidazole, TBDMSCl, DMF, rt, 3 h; (b) $C_2O_2Cl_2$, DCM, 0 °C to rt, 2 h; (c) DMAP, THF, rt, 4 h; (d) TBAF, AcOH, THF, 0 °C, 3 h.

an amine. Firstly, using the 4-(2-Aminoethyl) benzene-1,2-diol hydrochloride (Dopamine) as the initial substrate, 1-(3-Dimethylaminopropyl)-3-ethylcarbodiimide hydrochloride (EDCI) as condensation agent, 1-hydroxybenzotriazole (HOBt) as catalytic agent, and triethylamine as a base, Adamantaneacetic acid could couple with dopamine hydrochloride to afford amide compound **DP-ADM** in 74.6% yield as a white solid.[31] Mitochondrial oxidative stress is closely related to vascular endothelial cell function, which causes the dysfunction of vascular endothelial cells by inducing mitophagy, reducing nitric oxide production, inflammation, cellular metabolic imbalance and apoptosis.[32] Triphenylphosphonium (TPP[+]) is a lipophilic delocalized cation, generally referred to as "mitochondria-addressed"; it has been widely used to develop novel mitochondria-targeted cationic compounds, finely tuned to sequester bioactive molecules, such as antioxidants, probes and other pharmacophores, into the mitochondrial matrix.[31] Thus, combining the TPP[+] cation represents one of the most used synthetic strategies in the field, reinvented and refined by Murphy and coworkers.[33] (5-Carboxypentyl) triphenylphosphonium bromide 4 was subjected to a condensation reaction with dopamine hydrochloride, under the conditions of N, N'-dicyclohexylcarbodiimide (DCC) as the condensation agent and 4-dimethylaminopyridine (DMAP) as the catalytic agent, to afford amide compound **DP-TPP** in 26.8% yield as a white solid (Scheme 2).[34]

3.4-Dihydroxyphenylacetic acid (DOPAC) is a predominant biologically-active catabolite of quercetin glycosides and a major dopamine metabolite.[35] DOPAC protects against mitochondrial dysfunction.[36] Under the conditions of (benzo-triazol-1-yloxa) tris (dimethylamino)phosphonium hexafluorophosphate (BOP) as the condensation agent and triethyla-mine as a base, DOPAC was transferred to greater stability and lipophilicity amide compound **DOP-ADM** in 21.5% yield as a white solid (Scheme 3).[26]

Computational Analysis of Cell Permeability and Absorption

Cell permeability and absorption on compounds are much desired properties in drug discovery. Fast and reliable estimation of these properties is one of the key factors in accelerating the process of drug discovery and development. According to Lipinski's rule,[37] it is predicted that good membrane permeability or absorption is more likely to emerge under the conditions of CLog P ≤5, molecular weight ≤500, number of hydrogen bond acceptors (ON acceptors) ≤10, and number of hydrogen bond donors (OHNH donors)≤5. One violation of these parameters is acceptable If two of these
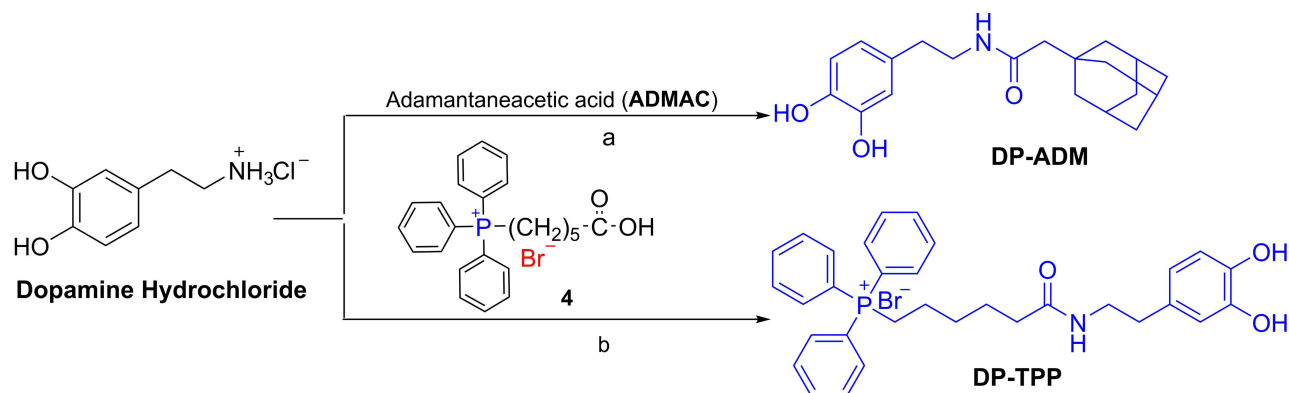
Scheme 2 Reagent and condition: (a) HOBT, EDCI, Et₃N, DCM, 0 °C to rt, overnight; (b) DMAP, DCC, DCM, rt, overnight.
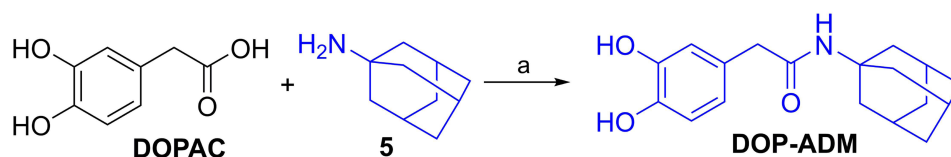
Scheme 3 Reagent and condition: (a) BOP, Et₃N, DMF/DCM, 0 °C to rt, overnight.

parameters are out of range, the alert value was set to 1, indicating a poor permeation. Among the tested compounds, it was observed that DP-TPP violated "Lipinski's Rule" (molecular weight beyond 500 and CLog P beyond 5) (Table 1). However, the computational alert does not allow a very favorable value of one parameter to compensate for a less favorable value of another parameter.[37]

Another very helpful parameter for the prediction of absorption and cell permeability is the molecular topographical polar surface area (tPSA), defined as the sum of surfaces of polar atoms in a molecule. The computational values of tPSA for the tested compounds are shown in Table 1 (ranging from 26.02 to 77.76 Å^2).[38] Magnitude of absorption is expressed by the percentage of absorption. Absorption percent (%ABS) was calculated using the expression: %ABS = 109–0.345 tPSA.[39] The absorption of all the tested compounds is greater than 80%. The results of theoretical studies suggested that these designed compounds can be used as further biological evaluation in the search for new therapeutic alternatives to treat vascular diseases.

DP-ADM Stood Out as a Potential Drug in Protecting the Endothelial Cells Against Lipid Overload

The cell viability was initially tested to examine the toxicity of HT derivatives in cultured endothelial cells. As shown in Figure 4A, except for high dose of HT-ADM and DOP-ADM (10 μM), other HT derivatives showed subtle effects on cell viability, suggesting low toxicity of these HT derivatives in endothelial cells. PA challenge was employed to induce lipotoxicity-associated endothelial dysfunction.[40,41] Endothelial cells were pretreated with HT derivatives (0.1, 1, 10 μM) for 24 h, followed by PA challenge (500 μM) for another 24 h. Existing literature suggests doses of HT ranging from 1 to 100 μM.[42–45] In our experiments, treatment of HAECs with 10 μM HT and HT-ADM resulted in reduced cell viability (Figure 4A). Therefore, we concluded that doses below 10 μM are associated with minimal cytotoxic effects, and at concentrations lower than 10 μM, both HT and its derivatives exhibit enhanced anti-inflammatory properties (Figure 4B and C). Consequently, we used the cell administration dosage range from 0.1 to 10 μM. Inflammation is the main factor participating in endothelial dysfunction. Inflammatory factors interleukin 6 (IL-6) and matrix metalloproteinase 1 (MMP-1) were drastically increased in response to PA challenge. HT and its derivates, DP-ADM, HT-ADM, and DP-TPP, decreased the MMP-1 transcription in endothelial cells with PA treatment (Figure 4B). However, in vitro, only HT derivative DP-ADM decreased IL-6 transcription in endothelial cells with PA treatment (Figure 4C). When compared to the model group (500 μM Palmitate), the DP-ADM treatment (0.1, 1, 10 μM) resulted in the following reductions for the MMP-1 levels: 51.4%, 66.5%, 44.7%. For IL-6 levels, the reductions were as follows: 77.2%, 69.3%, 28.4%. HT-ADM, DP-TPP, and DOP-ADM groups showed no reduction in the relative levels of IL-6 mRNA regardless of showing low cytotoxicity. This may be related to the chemical properties of the substances and their target. HT-ADM, DP-TPP, and DOP-ADM may possess unique chemical structures that hinder effective interactions with biomolecules regulating IL-6 expression. For instance, they might not penetrate specific cellular regions or may fail to bind with enzymes or regulatory factors associated with IL-6 gene transcription. The chemical structures of these substances may determine that they can only interact with certain cellular

Table 1 The Absorption and Permeability Studies for the Tested Compounds

Entry	MW[a]	CLogP[b]	n OHNH donors [c]	n ON acceptors [d]	Alert[e]	tPSA[f]	ABS%[g]
HT-ADM	330.42	5.33	2	2	0	66.76	85.97
DP-ADM	329.44	4.07	3	1	0	69.56	85.00
DP-TPP	592.51	6.78	3	1	1	69.56	85.00
DOP-ADM	301.39	2.08	3	1	0	69.56	85.00
DP	153.18	0.17	3	0	0	66.48	86.06
HT	154.16	0.07	3	0	0	60.69	88.06
ADMAA	194.27	4.12	1	1	0	37.3	96.13
DOPAC	168.15	0.15	3	1	0	77.76	82.17
ADMA	151.25	2.0	1	0	0	26.02	100.02
TPP	457.35	6.83	1	1	0	37.3	96.13

Notes: [a] Molecular weight of the tested compounds. [b] Calculated LogP. [c] Sum of OH and NH H-bond donors. [d] Sum of N and O H-bond acceptors. [e] Computational alert according to the rule of 5; 0, no problem detected; 1, poor absorption or permeation are more likely to emerge. [f] Topographical Polar surface area (PSA) (7.0–200 Å^2). [g] Percentage of absorption.
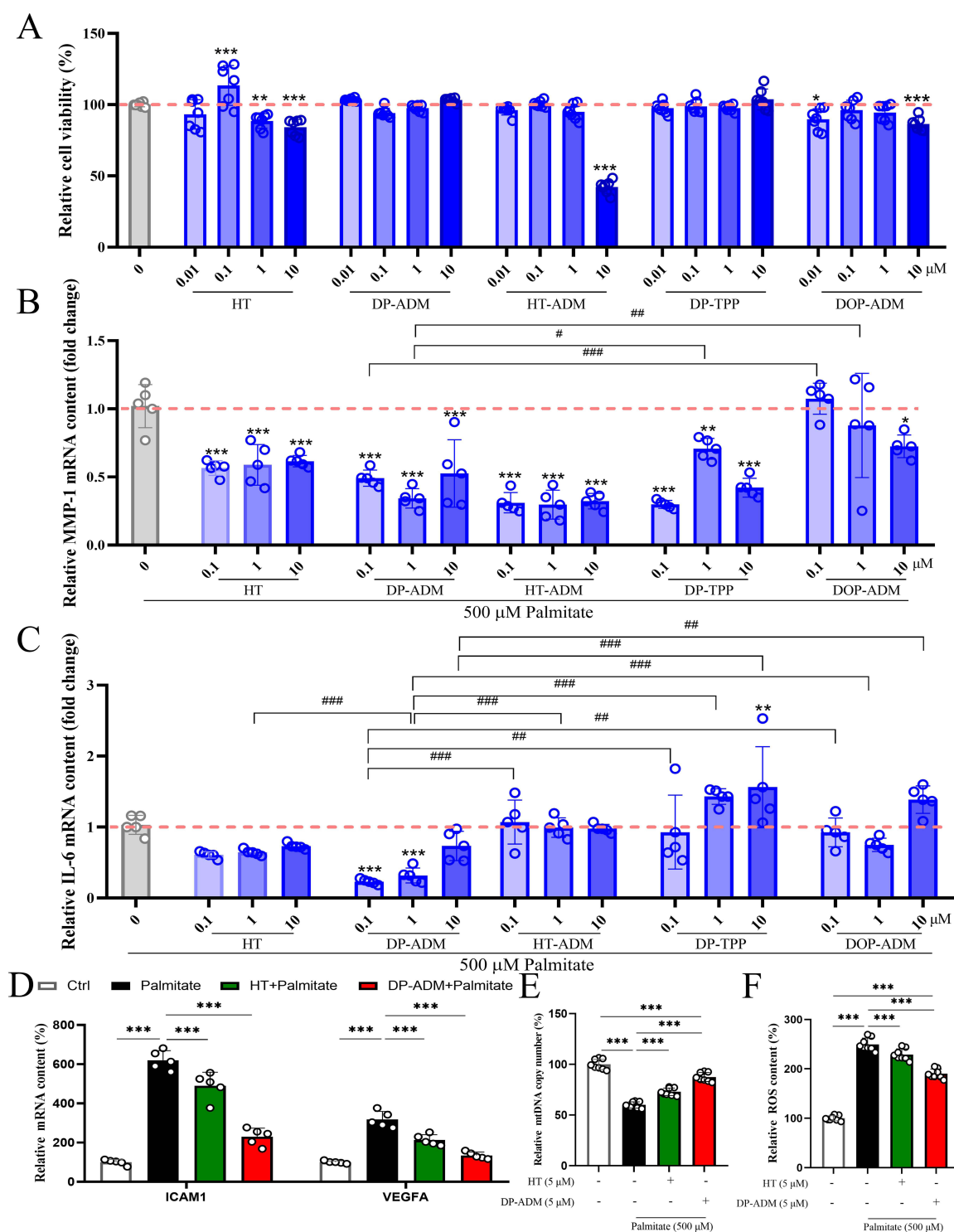
Figure 4 The Effects of HT derivatives on endothelial cells. (**A**) Except for high dose of HT-ADM and DOP-ADM (10 μM), other HT derivatives showed subtle effects on cell viability in endothelial cells. n=7. *, 0 vs other groups of HT derivatives at different concentrations. (**B**) The effects of HT and its derivatives on transcription of MMP-1 in endothelial cells with PA treatment. n=5. *, 0 vs other groups of HT derivatives at different concentrations. #, DP-ADM group at a specific concentration vs other groups of HT derivatives at the same concentration. (**C**) The effects of HT and its derivatives on transcription of IL-6 in endothelial cells with PA treatment. n=5. *, 0 vs other groups of HT derivatives at different concentrations. #, DP-ADM group at a specific concentration vs other groups of HT derivatives at the same concentration. (**D**) The effects of HT and DP-ADM on transcription of ICAM-1 and VEGFA in endothelial cells with PA treatment. n=5. (**E**) The effects of HT and DP-ADM on mtDNA copy number in endothelial cells with PA treatment. n=8. (**F**) The effects of HT and DP-ADM on ROS in endothelial cells with PA treatment. n=8. Data are presented as mean±SD, and differences were analyzed using one-way ANOVA. *, $^{#}$P<0.05, **, $^{##}$P<0.01, ***, $^{###}$P<0.001.

components, which are unrelated to the regulation of IL-6 expression, despite not causing cytotoxicity. According to Lipinski's rule,[37] it is predicted that good membrane permeability or absorption is more likely to emerge under the conditions of CLog P ≤5. Among the tested compounds, it was observed that The CLog P of DP-TPP and HT-ADM beyond 5 (Table 1). And DP-TPP violated "Lipinski's Rule" (molecular weight beyond 500 and CLog P beyond 5). What is more, the structurally difference of DP-ADM and HT-ADM are only ester and amide bonds. Therefore, the different metabolic pathways of ester and amide bonds may be one of the reasons for their different activities.[46] Although DP-ADM and DOP-ADM are similar in structure, the linking group of DP-ADM is longer than that of DOP-ADM, indicating that the spatial structure of the molecule is also an important factor affecting the activity.[47] Additionally, the expression of endothelial function-related protein markers, including ICAM1 and VEGFA, was assessed. Results indicated that PA exposure significantly elevated the levels of ICAM1 and VEGFA in human aortic endothelial cells (HAECs). Conversely, treatment with HT and DP-ADM notably reduced the expression of both markers, with DP-ADM demonstrating superior efficacy (Figure 4D). Furthermore, the levels of reactive oxygen species (ROS) associated with oxidative stress and mitochondrial function-related mtDNA content were assessed. It was similarly found that both hydroxytyrosol (HT) and DP-ADM could improve the alterations induced by PA in these parameters (Figure 4E and F). Thus, HT derivate DP-ADM stands out as a potential substitution of HT in the treatment of endothelial dysfunction.

DP-ADM Decreased Inflammation and Circulating Lipids in Mice With Hyperlipidemia

To investigate the potential benefits of DP-ADM on endothelial function in a content the context of hyperlipidemia, an acute hyperlipidemia-induced endothelial injury mouse model was used. This hyperlipidemia model was constructed by intraperitoneal injection of P407 (0.05 g/kg). P407 injection upregulated circulating lipids, including NEFA, TG, TC, and LDL-c, and down-regulated HDL-c, in mice (Figure 5A–G). Pretreatment with HT or DP-ADM showed no significant effects on body weight but decreased circulating NEFA, TG, TC, and LDL and increased circulating HDL in mice, suggesting that HT and DP-ADM lowers circulating lipids (Figure 5A–G). Additionally, in vivo, we also observed that HT and DP-ADM decreased circulating IL-6 and TNF-α, and DP-ADM exhibited a more obvious effect on lowering IL-6 and TNF-α in mice with hyperlipidemia (Figure 5H and I). These results suggested that DP-ADM decreased inflammation and circulating lipids in mice with hyperlipidemia.

DP-ADM Improved Endothelial Function in Mice With Hyperlipidemia

Endothelial function was then evaluated. Hyperlipidemia induced endothelial dysfunction, as evidenced by reduced contents of NOand reduced ACh-induced vasodilation in isolated thoracic aortas (Figure 6A–D). HT and DP-ADM increased the contents of NO in circulation and thoracic aortas (Figure 6A and B). However, only DP-ADM improved vasodilation in response to ACh in mice with hyperlipidemia, indicating an improvement of vascular endothelial cells (Figure 6C). Furthermore, DP-ADM decreased the thickness of thoracic aortas which was enlarged by P407 in mice with hyperlipidemia (Figure 6D and E), indicating an improvement in vascular structure. While HT showed subtle effects on the vascular structure remodeling (Figure 6D and E). These results suggested that DP-ADM is protective to endothelial dysfunction in mice with hyperlipidemia, and its effect on improving endothelial function is superior to HT.

DP-ADM Improved Endothelial Function Through Inactivation of p38 Signaling

The p38 mitogen-activated protein kinases (MAPKs) play a pivotal role in responding to lipid overload and inflammation through activation of NF-κB signaling.[48] PA activated p38/NF-κB signaling as evidenced by increased phosphorylation of p38 and NF-κB (Figure 7A and B). DP-ADM treatment attenuated the activation of p38/NF-κB signaling in PA-treated endothelial cells, while HT exhibited little effects on p38/NF-κB signaling activation (Figure 7A and B). Importantly, the inhibition of p38 MAPK signaling through the use of SB203580, a potent inhibitor, in combination with DP-ADM significantly reduces the expression of IL-6 and MMP-1 more effectively than DP-ADM alone (Figure 7C–F). Additionally, the inhibition of NF-κB using QNZ, a quinazoline derivative, in combination with DP-ADM significantly reduces the expression of IL-6 and MMP-1 more effectively than DP-ADM alone (Figure 7G and H). These results suggested that DP-ADM inhibits endothelial inflammation through the inhibition of the p38/NF-κB signaling pathway.
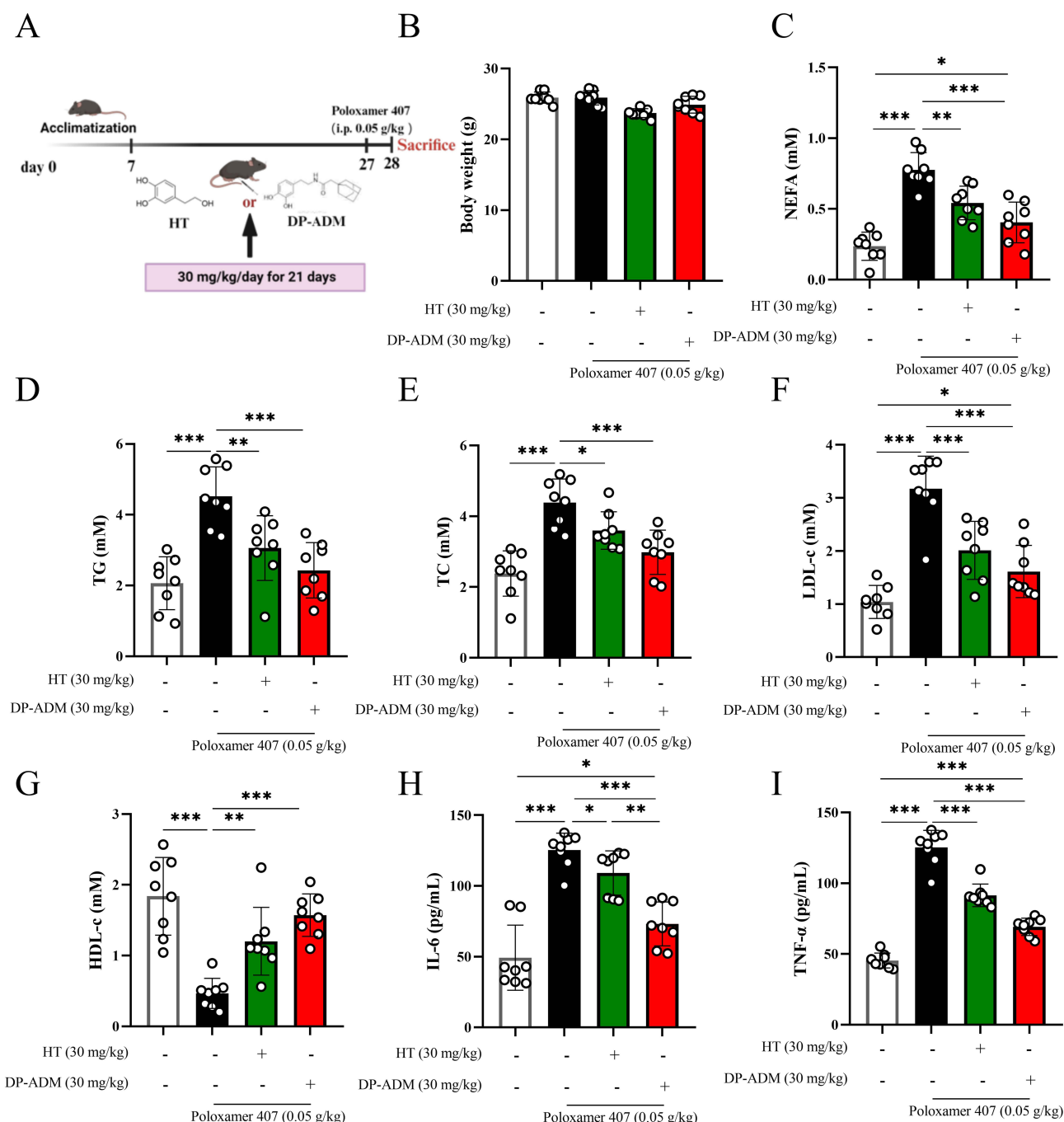
Figure 5 DP-ADM decreased inflammation and circulating lipids in mice with hyperlipidemia. (**A**) An acute hyperlipidemia-induced endothelial injury mouse model was used to investigate the potential benefits of DP-ADM on endothelial function. (**B**) Body weight of mice with hyperlipidemia. (**C–G**) Circulating lipids, including NEFA (**C**), TG (**D**), TC (**E**), and LDL-c (**F**), and HDL-c (**G**), in mice. (**H**) Circulating IL-6 in mice. (**I**) Circulating TNF-α in mice. n=8. Data are presented as mean±SD, and differences were analyzed using one-way ANOVA. *P<0.05, **P<0.01, ***P<0.001.

DP-ADM Improved Endothelial Function Through Inactivation of Erk Signaling

Erk is one of the other MAPK subfamilies. Next, we also tested the role of Erk signaling in the anti-inflammatory effect of DP-ADM. PA activated Erk signaling as evidenced by increased phosphorylation of Erk and the downstream signal p-eNOS/eNOS, and decreased the expression of FoxO1 (Figure 8A and B). HT and DP-ADM treatments attenuated the activation of Erk signaling, as evidenced by decreasing p-Erk/Erk and p-eNOS/eNOS, in PA-treated endothelial cells (Figure 8A and B). Specifically, only DP-ADM increased the expression of FoxO1 in endothelial cells with PA treatment
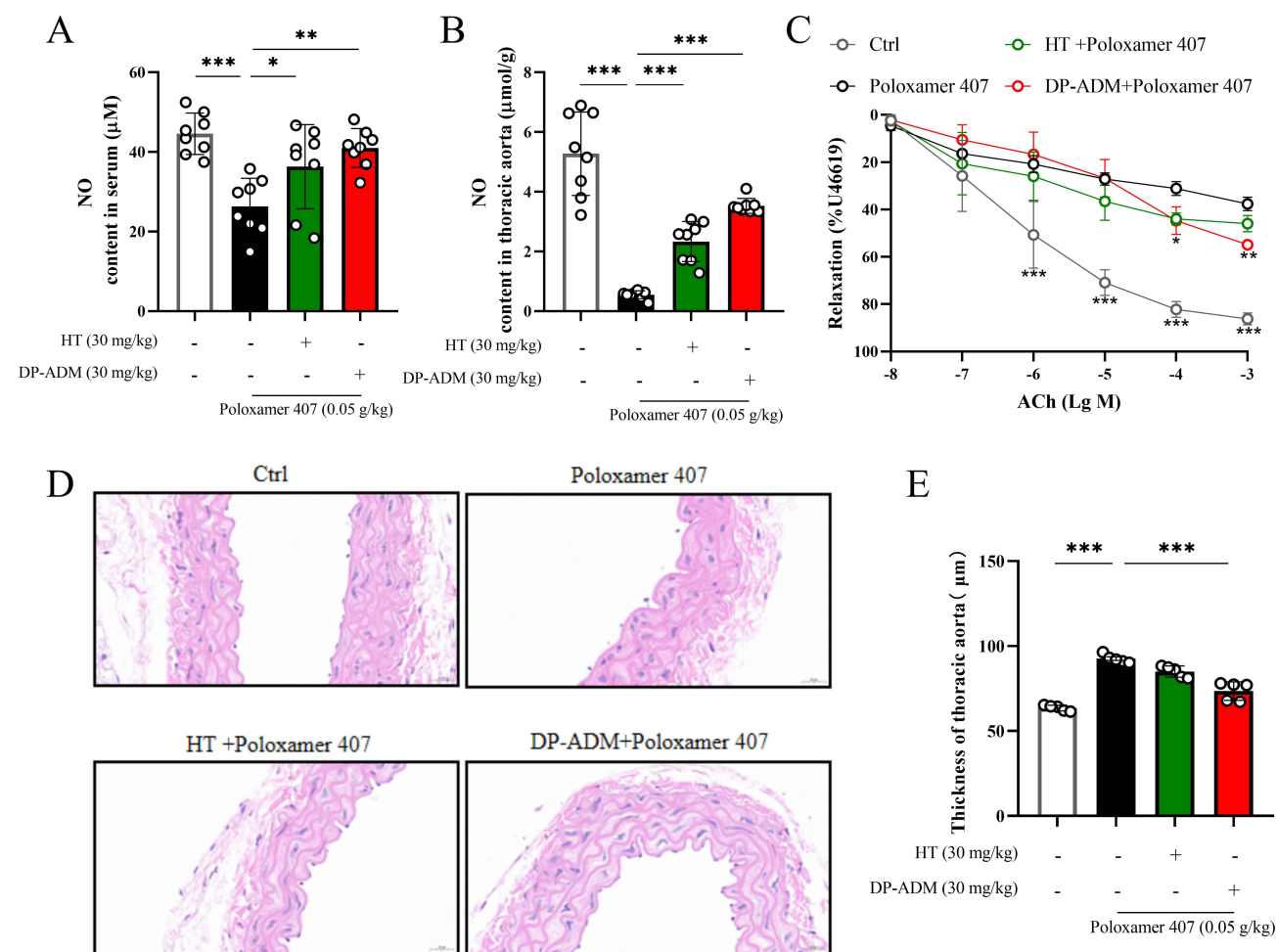
Figure 6 DP-ADM improved endothelial function in mice with hyperlipidemia. (**A** and **B**) HT and DP-ADM increased the contents of NO in circulation (**A**) and thoracic aortas (**B**) in mice with hyperlipidemia. n=8. (**C**) DP-ADM improved vasodilation in response to ACh in isolated aortas from mice with hyperlipidemia. n=5. (**D** and **E**) DP-ADM decreased the thickness of thoracic aortas in mice with hyperlipidemia. Typical H&E images (**D**) and the quantified results (**E**) were shown. n=5. Data are presented as mean±SD, and differences were analyzed using one-way ANOVA (**A**, **B**, and **E**) or two-way ANOVA (**C**). *P<0.05, **P<0.01, ***P<0.001.

(Figure 8A and B). In fact, DP-ADM increased the FoxO1 translocation to nucleus, and U0126, an Erk inhibitor, abolished the effect of DP-ADM on the promotion of FoxO1 translocation to nucleus (Figure 8C and D). It is reported that FoxO1 signaling regulates mitochondrial function.[41,49] As mitochondria play a critical role in the regulation of endothelial function and FoxO1 signaling is involved in the regulation of mitochondrial function,[4] mitochondria biogenesis and dynamics-related proteins were detected. PA decreased the expression of PGC-1α, a key regulator of mitochondria biogenesis, and HT and DP-ADM upregulated the expression of PGC-1α, while other mitochondrial dynamic-related proteins were not changed upon HT and DP-ADM treatments in endothelial cells with PA challenge (Figure 8E and F). These results suggested that DP-ADM improves endothelial function through activation of Erk signaling.

Discussion

HT is a natural phenolic compound with protective effects against endothelial cell dysfunction.[12] It is well-known that HT possesses the ability to prevent oxidation and has been identified as a potential candidate for regulating inflammation.[50] However, the hydrophilic nature of HT strongly limited its oral bioavailability due to an insufficient uptake from the mucosa resulting from its poor epithelial permeability.[15,16] In addition, phenolic compounds are unstable in air and oxygen.[17] To increase the absorption and stability of HT and improve its beneficial effect against endothelial dysfunction, we employed the pharmacophore connection strategy to design and synthesize 4 novel types of
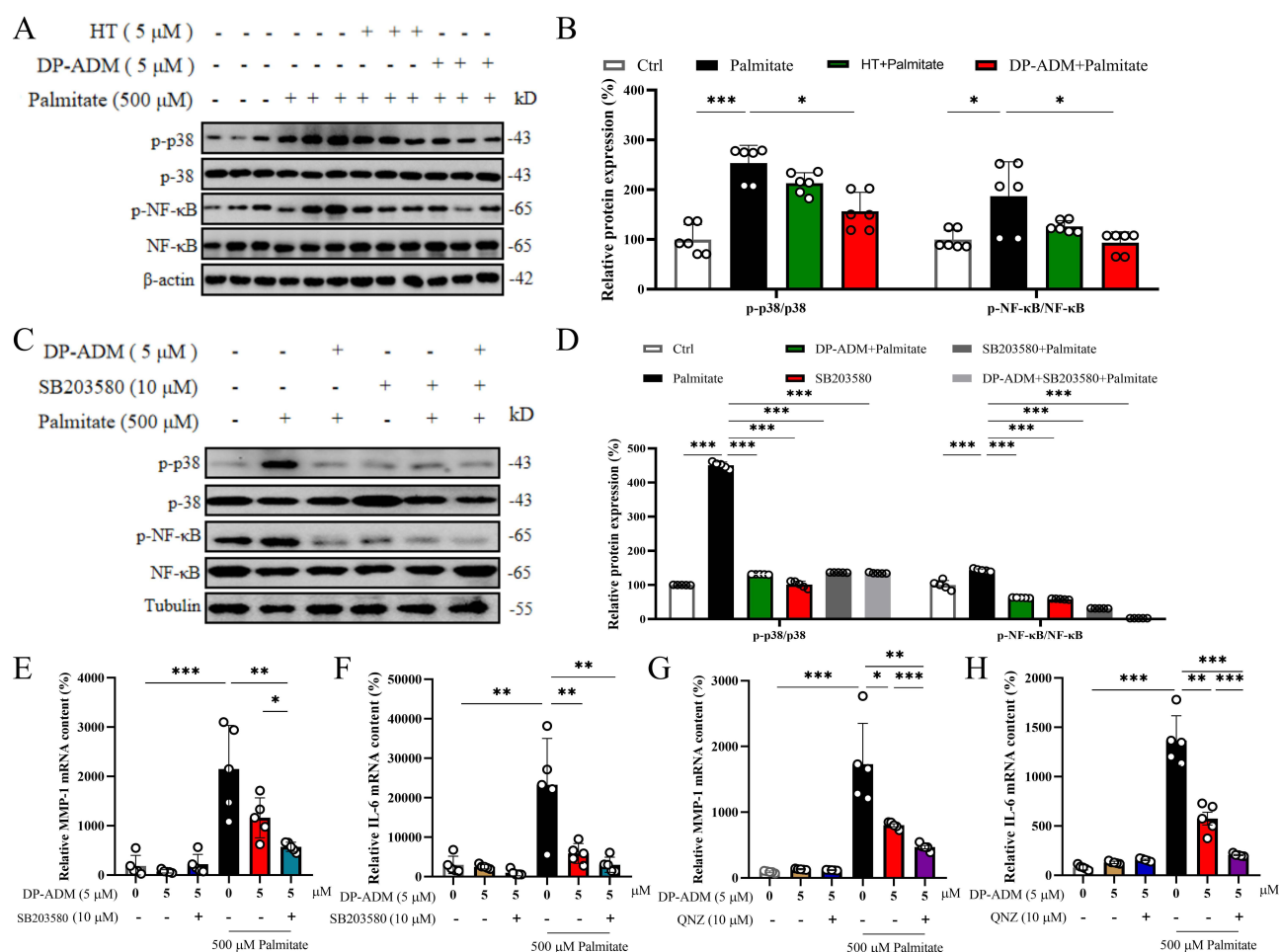
Figure 7 DP-ADM improved endothelial function through activation of p38 signaling. (**A and B**) DP-ADM treatment attenuated the activation of p38/NF-κB signaling in PA-treated endothelial cells. Typical WB images (**A**) and the quantified results (**B**) were shown. n=6. C-F. Inhibition of p38 MAPK signaling through the use of SB203580, a potent inhibitor, in combination with DP-ADM significantly reduces the expression of IL-6 and MMP-1 more effectively than DP-ADM alone. Typical WB images were shown in (**C**) and the quantified results (**D**) were shown. n=5. Transcription of MMP-1 (**E**) and IL-6 (**F**) were shown. n=5. G-H. Inhibition of NF-κB using QNZ, a quinazoline derivative, in combination with DP-ADM significantly reduces the expression of IL-6 and MMP-1 more effectively than DP-ADM alone. Transcription of MMP-1 (**G**) and IL-6 (**H**) were shown. n=5. Data are presented as mean±SD, and differences were analyzed using one-way ANOVA. *P<0.05, **P<0.01, ***P<0.001.

hydroxytyrosol derivatives, including HT-ADM, DP-ADM, DP-TPP and DOP-ADM. Among these HT derivatives, DP-ADM stood out as a potential drug in protecting the endothelial cells against lipid overload. The structural difference between HT-ADM and DP-ADM is that the former contains ester bonds and the latter contains amide bonds, indicating that the amide functional group may be a better pharmacophore.[30,51] These results suggest that the stereochemical structure and linking groups, in addition to pharmacophore, may affect their potency by inhibiting certain target molecules and signaling pathways, or pharmacokinetics.

The effects of the synthesized compounds on endothelial function were tested in both cultured HAECs and mice with hyperlipidemia. Almost all these compounds showed no significant effects on cell viability in cultured HAECs, except for HT-ADM and DOP-ADM which decreased cell viability at a concentration of 10 μM. The four synthesized compounds were initially investigated for their inhibitory effects on the production of MMP-1 and IL-6 in response to lipid overload in HAECs. The results showed that the production of MMP-1 and IL-6 were significantly inhibited by DP-ADM. Compared with HT and its derivatives HT-ADM, DP-TPP and DOP-ADM, DP-ADM showed a potent inhibitory effect on inflammatory cytokines MMP-1 and IL-6, suggesting that ADM is a better pharmacophore than triphenylphosphonium. Although triphenylphosphonium (TPP⁺) has been widely used to develop novel mitochondria-targeted cationic compounds, finely tuned to sequester bioactive molecules, such as antioxidants, probes and other pharmacophores, into the mitochondrial matrix,[31] DP-ADM showed a more superior effect than HT in lowering inflammatory

Figure 8 DP-ADM improved endothelial function through activation of Erk signaling. (**A and B**) HT and DP-ADM treatments attenuated the activation of Erk signaling, as evidenced by decreasing p-Erk/Erk and p-eNOS/eNOS ratio, in PA-treated endothelial cells. Typical WB images (**A**) and the quantified results (**B**) were shown. n=6. C-D. DP-ADM increased the FoxO1 translocation to nucleus, and U0126, a Erk inhibitor, abolished the effect of DP-ADM on promotion of FoxO1 translocation to nucleus. Typical fluorescent images (**C**) and the quantified results (**D**) were shown. n=28 control cell, 23 for DP-ADM cell, 62 for U0126 cell and 41 for DP-ADM+U0126 cell. E-F. HT and DP-ADM upregulated the expression of PGC-1α, while other mitochondrial dynamic-related proteins were not changed upon HT and DP-ADM treatments in endothelial cells with PA challenge. Typical WB images (**E**) and the quantified results (**F**) were shown. n=6. Data are presented as mean±SD, and differences were analyzed using one-way ANOVA. *$P < 0.05$, **$P < 0.01$, ***$P < 0.001$.

cytokines and improving endothelial function in mice with hyperlipidemia. These results suggested that DP-ADM is a substitute for HT, which is more efficient in improving endothelial function.

The healthy endothelium controls vascular homeostasis by modulating vascular tone, maintaining blood fluidity and flow, controlling vessel wall permeability, and counteracting vascular inflammation.[1] As such, endothelial dysfunction is essential in the initiation and progression of various diseases, including atherosclerosis, heart failure, and metabolic diseases.[52–54] It is well established that hyperlipidemia is one of the major risk factors in inducing endothelial dysfunction.[40,55] Lipid overload induces oxidative stress, inflammation, mitochondrial dysfunction, and cell death in

endothelial cells.[56,57] Thus, targeting endothelial cells or lipids is a well-accepted strategy in the prevention and treatment of both cardiovascular diseases and metabolic diseases.[40] In our study, we showed that PA challenge induced upregulation of inflammatory cytokines, MMP-1 and IL-6, and DP-ADM decreased PA-induced inflammation both in vivo and in vitro. MAPKs, which belong to a large family of serine-threonine kinases, play a pivotal role in responding to metabolic disturbance.[58] Extracellular factors activate members of the major MAPK subfamilies, including p38 and Erk. In conjunction with NF-κB activation, MAPK activation induces the expression of immune response genes and cell death pathway-related genes.[59] Consistently, we observed that PA treatment activated p38 and Erk signaling, as well as NF-κB signaling, which were inhibited by DP-ADM. Specifically, DP-ADM exerts benefits against lipid overload through inhibition of MAPK signaling. Additionally, we identified FoxO1 as a downstream signal of MAPK, which is activated by DP-ADM. FoxO1 activation is accompanied by an improvement in mitochondrial biogenesis. It is reported that FoxOs regulate mitochondrial biogenesis by inhibiting nuclear respiratory factor 1- transcription factor A, mitochondrial signaling directly.[60]

Conclusion and Limitation

Four HT derivatives (HT-ADM, DP-ADM, DP-TPP, DOP-ADM) were created to improve HT's biological effects. Among them, DP-ADM was the most effective in reducing inflammation and lowering lipids in high-fat conditions. It works by blocking MAPK signaling and activating FoxO1 signaling. These findings suggest that DP-ADM could help improve endothelial function in metabolic diseases. However, in vivo confirmation of the proposed mechanism through which DP-ADM improves endothelial function, in addition to IL-6 measurements, is essential, particularly regarding the involvement of the p38 MAPK and ERK signaling pathways. Although the P407-induced acute hyperlipidemia model has been widely used in research, it represents an acute disease model. Future studies should further investigate the role and mechanism of DP-ADM in obesity induced by a long-term high-fat diet to better assess its translational potential. Additionally, the bioavailability, absorption, stability, and pharmacokinetic profile of these novel HT derivatives should be evaluated in the future. This will provide a stronger foundation for the subsequent translational application of DP-ADM.

Abbreviations

Ach, Acetylcholine; ADM, Adamantane; ADMA, Adamantan-1-amine; ADMAA, Adamantane acetic acid; BOP, (benzotriazol-1-yloxa) tris (dimethylamino)phosphonium hexafluorophosphate; d, Doublet; DCC, Dicyclohexylcarbodiimide; DCM, Dichloromethane; DHE, Dihydroethidium; DMAP, 4-dimethylaminopyridine; DMEM, Dulbecco's modified Eagle's medium; DMSO, Dimethyl sulphoxide; Dopamine, 4-(2-Aminoethyl) benzene-1,2-diol hydrochloride; DOPAC, 3.4-Dihydroxyphenylacetic acid; DP, Dopamine; EDCI, 1-ethyl-3(3-dimethylpropylamine) carbodiimide; EtOA, Ethyl acetate; FBS, Fetal bovine serum; HAECs, Human aorta endothelial cells; HDL-c, High-density lipoprotein cholesterol; HE, Hematoxylin & Eosin; HOBt, 1-hydroxybenzotriazole; HT, Hydroxytyrosol; IL-6, Interleukin 6; i.p, Intraperitoneally; LDL-c, Low-density lipoprotein cholesterol; m, Multiplet (spectral); MAPKs, Mitogen-activated protein kinases; MMP-1, Matrix metalloproteinase 1; MTT, 3-[4,5-dimethylthiazol-2-yl]-2,5 diphenyl tetrazolium bromide; NEFA, non-esterified fatty acid; PA, Palmitic acid; PBS, Phosphate buffered saline; PE, Petroleum ether; P407, Poloxamer 407; q, Quartet; ROS, Reactive Oxygen Species; s, Singlet; SD, Standard deviation; SDS-PAGE, SDS-polyacrylamide gel electrophoresis; t, Triplet; TBDMSCl, Tert-butyldimethylsilyl chloride; TBHP, Tert-Butyl hydroperoxide; TC, Total cholesterol; TG, Triglyceride; THF, Tetrahydrofuran; TNF-α, Tumor necrosis factor-α; TPP$^+$, Triphenylphosphonium; TPP, (5-carboxypentyl) triphenylphosphonium bromide; Tpsa, Topographical polar surface area.

Ethical Approval

All animal procedures were approved by Animal Experiment Welfare and Ethics Committee of Fourth Military Medical University (NO. IACUC-2023075).

Acknowledgments

Zhang, a professional English teacher in Xi'an Technology University, for English language edits of the manuscript. This work was financially supported by a basic research program of natural science in Shaanxi province (2017JZ023) and the National Natural Science Foundation of China (32100917).

Disclosure

The authors have declared no conflict of interest.

References

1. Augustin HG, Koh GY. A systems view of the vascular endothelium in health and disease. *Cell*. 2024;187(18):4833–4858. doi:10.1016/j.cell.2024.07.012
2. Bloom SI, Islam MT, Lesniewski LA, et al. Mechanisms and consequences of endothelial cell senescence. *Nat Rev Cardiol*. 2023;20(1):38–51. doi:10.1038/s41569-022-00739-0
3. Li G, Xu K, Xing W, et al. Swimming exercise alleviates endothelial mitochondrial fragmentation via inhibiting dynamin-related protein-1 to improve vascular function in hypertension. *Hypertension*. 2022;79(10):e116–e128. doi:10.1161/HYPERTENSIONAHA.122.19126
4. Zhang X, Gao F. Exercise improves vascular health: role of mitochondria. *Free Radic Biol Med*. 2021;177:347–359. doi:10.1016/j.freeradbiomed.2021.11.002
5. Zaric B, Obradovic M, Trpkovic A, et al. Endothelial dysfunction in dyslipidaemia: molecular mechanisms and clinical implications. *Curr Med Chem*. 2020;27(7):1021–1040. doi:10.2174/0929867326666190903112146
6. Zhang Y, Li JJ, Xu R, et al. Nogo-B mediates endothelial oxidative stress and inflammation to promote coronary atherosclerosis in pressure-overloaded mouse hearts. *Redox Biol*. 2023;68:102944. doi:10.1016/j.redox.2023.102944
7. Yang L, Zhang J, Xing W, et al. SIRT3 deficiency induces endothelial insulin resistance and blunts endothelial-dependent vasorelaxation in mice and human with obesity. *Sci Rep*. 2016;6:23366. doi:10.1038/srep23366
8. Wang L, Luo JY, Li B, et al. Integrin-YAP/TAZ-JNK cascade mediates atheroprotective effect of unidirectional shear flow. *Nature*. 2016;540 (7634):579–582. doi:10.1038/nature20602
9. Xu S, Ilyas I, Little PJ, et al. Endothelial dysfunction in atherosclerotic cardiovascular diseases and beyond: from mechanism to pharmacotherapies. *Pharmacol Rev*. 2021;73(3):924–967. doi:10.1124/pharmrev.120.000096
10. Bertelli M, Kiani AK, Paolacci S, et al. Hydroxytyrosol: a natural compound with promising pharmacological activities. *J Biotechnol*. 2020;309:29–33. doi:10.1016/j.jbiotec.2019.12.016
11. Britton J, Davis R, O'Connor KE. Chemical, physical and biotechnological approaches to the production of the potent antioxidant hydroxytyrosol. *Appl Microbiol Biotechnol*. 2019;103(15):5957–5974. doi:10.1007/s00253-019-09914-9
12. Lopez-Jimenez A, Gallardo E, Espartero JL, et al. Comparison of the anti-angiogenic potential of hydroxytyrosol and five derivatives. *Food Funct*. 2018;9(8):4310–4316. doi:10.1039/c8fo01140k
13. Christodoulou A, Nikolaou PE, Symeonidi L, et al. Cardioprotective potential of oleuropein, hydroxytyrosol, oleocanthal and their combination: unravelling complementary effects on acute myocardial infarction and metabolic syndrome. *Redox Biol*. 2024;76:103311. doi:10.1016/j.redox.2024.103311
14. Zodio S, Serreli G, Melis MP, et al. Protective effect of hydroxytyrosol and tyrosol metabolites in LPS-induced vascular barrier derangement in vitro. *Front Nutr*. 2024;11:1350378. doi:10.3389/fnut.2024.1350378
15. Freiria-Gandara J, Martinez-Senra T, Bravo-Diaz C. Exploring the use of hydroxytyrosol and some of its esters in food-grade nanoemulsions: establishing connection between structure and efficiency. *Antioxidants (Basel)*. 2023;12(11):2002. doi:10.3390/antiox12112002
16. Vilaplana-Perez C, Aunon D, Garcia-Flores LA, et al. Hydroxytyrosol and potential uses in cardiovascular diseases, cancer, and AIDS. *Front Nutr*. 2014;1:18. doi:10.3389/fnut.2014.00018
17. Marrero AD, Quesada AR, Martinez-Poveda B, et al. Anti-cancer, anti-angiogenic, and anti-atherogenic potential of key phenolic compounds from virgin olive oil. *Nutrients*. 2024;16(9):1283. doi:10.3390/nu16091283
18. Ragshaniya A, Kumar V, Tittal RK, et al. Nascent pharmacological advancement in adamantane derivatives. *Arch Pharm (Weinheim)*. 2024;357(3): e2300595. doi:10.1002/ardp.202300595
19. Doggrell SA. New drugs being developed for the treatment of tuberculosis. *Expert Opin Investig Drugs*. 2005;14(7):917–920. doi:10.1517/13543784.14.7.917
20. Mugnaini C, Rabbito A, Brizzi A, et al. Synthesis of novel 2-(1-adamantanylcarboxamido) thiophene derivatives. Selective cannabinoid type 2 (CB2) receptor agonists as potential agents for the treatment of skin inflammatory disease. *Eur J Med Chem*. 2019;161:239–251. doi:10.1016/j.ejmech.2018.09.070
21. Liang J, Zhang P, Yang H, et al. Design, synthesis and biological evaluation of novel nitric oxide donors with antioxidative activity. *Eur J Med Chem*. 2022;236:114331. doi:10.1016/j.ejmech.2022.114331
22. Singh AK, Kumar A, Singh H, et al. Concept of hybrid drugs and recent advancements in anticancer hybrids. *Pharmaceuticals (Basel)*. 2022;15 (9):1071. doi:10.3390/ph15091071
23. Martelli A, Testai L, Anzini M, et al. The novel anti-inflammatory agent VA694, endowed with both NO-releasing and COX2-selective inhibiting properties, exhibits NO-mediated positive effects on blood pressure, coronary flow and endothelium in an experimental model of hypertension and endothelial dysfunction. *Pharmacol Res*. 2013;78:1–9. doi:10.1016/j.phrs.2013.09.008
24. Lauretani F, Giallauria F, Testa C, et al. Dopamine pharmacodynamics: new Insights. *Int J mol Sci*. 2024;25(10):5293. doi:10.3390/ijms25105293
25. Benes FM. Carlsson and the discovery of dopamine. *Trends Pharmacol Sci*. 2001;22(1):46–47. doi:10.1016/s0165-6147(00)01607-2
26. Dizdar M, Vidic D, Požgan F, et al. Acetylcholinesterase inhibition and antioxidant activity of *N-trans*-Caffeoyldopamine and *N-trans*-Feruloyldopamine. *Sci Pharm*. 2018;86(2):11. doi:10.3390/scipharm86020011
27. Larsen EM, Johnson RJ. Microbial esterases and ester prodrugs: an unlikely marriage for combating antibiotic resistance. *Drug Dev Res*. 2019;80 (1):33–47. doi:10.1002/ddr.21468

28. Beaumont K, Webster R, Gardner I, et al. Design of ester prodrugs to enhance oral absorption of poorly permeable compounds: challenges to the discovery scientist. *Curr Drug Metab*. 2003;4(6):461–485. doi:10.2174/1389200033489253

29. Shinohara H, Saito H, Homma H, et al. N–H insertion reaction via an iron carbenoid from α-diazophenylpropionate and its application to the formal total synthesis of stizolobinic acid. *Tetrahedron*. 2020;76(46):131619. doi:10.1016/j.tet.2020.131619

30. Narendar Reddy T, Beatriz A, Jayathirtha Rao V, et al. Carbonyl compounds' journey to amide bond formation. *Chem Asian J*. 2019;14 (3):344–388. doi:10.1002/asia.201801560

31. Testai L, Sestito S, Martelli A, et al. Synthesis and pharmacological characterization of mitochondrial K$_{ATP}$ channel openers with enhanced mitochondriotropic effects. *Bioorg Chem*. 2021;107:104572. doi:10.1016/j.bioorg.2020.104572

32. Wang Y, Wu J, Wang J, et al. Mitochondrial oxidative stress in brain microvascular endothelial cells: triggering blood-brain barrier disruption. *Mitochondrion*. 2023;69:71–82. doi:10.1016/j.mito.2023.01.007

33. Murphy MP, Smith RA. Targeting antioxidants to mitochondria by conjugation to lipophilic cations. *Annu Rev Pharmacol Toxicol*. 2007;47:629–656. doi:10.1146/annurev.pharmtox.47.120505.105110

34. Tsandi E, Kokotos CG, Kousidou S, et al. Sulfonamides of homoproline and dipeptides as organocatalysts for Michael and aldol reactions. *Tetrahedron*. 2009;65(7):1444–1449. doi:10.1016/j.tet.2008.12.008

35. Tang Y, Nakashima S, Saiki S, et al. 3,4-Dihydroxyphenylacetic acid is a predominant biologically-active catabolite of quercetin glycosides. *Food Res Int*. 2016;89(Pt 1):716–723. doi:10.1016/j.foodres.2016.09.034

36. Catalán M, Ferreira J, Carrasco-Pozo C. The microbiota-derived metabolite of quercetin, 3,4-dihydroxyphenylacetic acid prevents malignant transformation and mitochondrial dysfunction induced by hemin in colon cancer and normal colon epithelia cell lines. *Molecules*. 2020;25 (18):4138. doi:10.3390/molecules25184138

37. Lipinski CA, Lombardo F, Dominy BW, et al. Experimental and computational approaches to estimate solubility and permeability in drug discovery and development settings. *Adv Drug Deliv Rev*. 2001;46(1–3):3–26. doi:10.1016/s0169-409x(00)00129-0

38. Herrera-R A, Castrillón W, Pastrana M, et al. Promising hybrids derived from S-Allylcysteine and NSAIDs Fragments against Colorectal Cancer: synthesis, *In-vitro* Evaluation, Drug-Likeness and *In-silico* ADME/tox Studies. *Iran J Pharm Res*. 2021;20(3):351–367. doi:10.22037/ijpr.2020.114347.14806

39. Zhao YH, Abraham MH, Le J, et al. Rate-limited steps of human oral absorption and QSAR studies. *Pharm Res*. 2002;19(10):1446–1457. doi:10.1023/a:1020444330011

40. Boutagy NE, Singh AK, Sessa WC. Targeting the vasculature in cardiometabolic disease. *J Clin Invest*. 2022;132(6):e148556. doi:10.1172/JCI148556

41. Liu X, Cao K, Lv W, et al. Punicalagin attenuates endothelial dysfunction by activating FoxO1, a pivotal regulating switch of mitochondrial biogenesis. *Free Radic Biol Med*. 2019;135:251–260. doi:10.1016/j.freeradbiomed.2019.03.011

42. Zrelli H, Wu CW, Zghonda N, et al. Combined treatment of hydroxytyrosol with carbon monoxide-releasing molecule-2 prevents TNF α-induced vascular endothelial cell dysfunction through NO production with subsequent NFκB inactivation. *Biomed Res Int*. 2013;2013:912431. doi:10.1155/2013/912431

43. Catalán Ú, López de Las Hazas MC, Rubió L, et al. Protective effect of hydroxytyrosol and its predominant plasmatic human metabolites against endothelial dysfunction in human aortic endothelial cells. *Mol Nutr Food Res*. 2015;59(12):2523–2536. doi:10.1002/mnfr.201500361

44. Abate M, Pisanti S, Caputo M, et al. 3-hydroxytyrosol promotes angiogenesis in vitro by stimulating endothelial cell migration. *Int J mol Sci*. 2020;21(10):3657. doi:10.3390/ijms21103657

45. Muñoz-Marín J, De la Cruz JP, Reyes JJ, et al. Hydroxytyrosyl alkyl ether derivatives inhibit platelet activation after oral administration to rats. *Food Chem Toxicol*. 2013;58:295–300. doi:10.1016/j.fct.2013.04.045

46. Nagaoka M, Sakai Y, Nakajima M, et al. Role of carboxylesterase and arylacetamide deacetylase in drug metabolism, physiology, and pathology. *Biochem Pharmacol*. 2024;223:116128. doi:10.1016/j.bcp.2024.116128

47. Qin XY, Chen BY, Fu JJ, et al. Synthesis, cytotoxicity and inhibition of NO production of ivangustin enantiomer analoguesues. *Eur J Med Chem*. 2015;102:256–265. doi:10.1016/j.ejmech.2015.07.051

48. Chowdhury A, Roy S, Chakraborti T, et al. Activation of proMMP-2 by U46619 occurs via involvement of p (38) MAPK-NFκB-MT1MMP signaling pathway in pulmonary artery smooth muscle cells. *mol Cell Biochem*. 2014;385(1–2):53–68. doi:10.1007/s11010-013-1814-4

49. Gao J, Liu X, Wang M, et al. Adenosine protects cardiomyocytes against acrolein-induced cardiotoxicity by enhancing mitochondrial homeostasis, antioxidant defense, and autophagic flux via ERK-activated FoxO1 upregulation. *Ecotoxicol Environ Saf*. 2024;283:116799. doi:10.1016/j.ecoenv.2024.116799

50. Batarfi WA, Yunus MHM, Hamid AA, et al. Hydroxytyrosol: a promising therapeutic agent for mitigating inflammation and apoptosis. *Pharmaceutics*. 2024;16(12):1504. doi:10.3390/pharmaceutics16121504

51. Yan Y, Jiang W, Liu L, et al. Dopamine controls systemic inflammation through inhibition of NLRP3 inflammasome. *Cell*. 2015;160(1–2):62–73. doi:10.1016/j.cell.2014.11.047

52. Soehnlein O, Libby P. Targeting inflammation in atherosclerosis - from experimental insights to the clinic. *Nat Rev Drug Discov*. 2021;20 (8):589–610. doi:10.1038/s41573-021-00198-1

53. Shan SK, Lin X, Wu F, et al. Vascular wall microenvironment: endothelial cells original exosomes mediated melatonin-suppressed vascular calcification and vascular ageing in a m6A methylation dependent manner. *Bioact Mater*. 2024;42:52–67. doi:10.1016/j.bioactmat.2024.08.021

54. Chang TT, Li YZ, Mo HW, et al. Inhibition of CCL7 improves endothelial dysfunction and vasculopathy in mouse models of diabetes mellitus. *Sci Transl Med*. 2024;16(763):eadn1507. doi:10.1126/scitranslmed.adn1507

55. Ceriello A, Taboga C, Tonutti L, et al. Evidence for an independent and cumulative effect of postprandial hypertriglyceridemia and hyperglycemia on endothelial dysfunction and oxidative stress generation: effects of short- and long-term simvastatin treatment. *Circulation*. 2002;106 (10):1211–1218. doi:10.1161/01.cir.0000027569.76671.a8

56. Pandey N, Anand SK, Kaur H, et al. Enhanced venous thrombosis and hypercoagulability in murine and human metabolic dysfunction-associated steatohepatitis. *J Thromb Haemost*. 2024;22(12):3572–3580. doi:10.1016/j.jtha.2024.08.023

57. Wu YW, Chen JW, Tsai HY, et al. Inhibition of adipocyte-derived FABP4 reduces adipocyte inflammation, improves angiogenesis, and facilitates wound healing in metabolic dysfunctions. *J Invest Dermatol*. 2024;S0022-202X (24)02086-4:1–18. doi:10.1016/j.jid.2024.08.017

58. Fang JY, Richardson BC. The MAPK signalling pathways and colorectal cancer. *Lancet Oncol*. 2005;6(5):322–327. doi:10.1016/S1470-2045(05)70168-6

59. Ando M, Magi S, Seki M, et al. Author Correction: iκBα is required for full transcriptional induction of some NFκB-regulated genes in response to TNF in MCF-7 cells. *NPJ Syst Biol Appl*. 2022;8(1):26. doi:10.1038/s41540-022-00239-4

60. Cheng Z. FoxO transcription factors in mitochondrial homeostasis. *Biochem J*. 2022;479(4):525–536. doi:10.1042/BCJ20210777